Global long-range transport and lung cancer risk from polycyclic aromatic hydrocarbons shielded by coatings of organic aerosol

Manish Shrivastava[a,1], Sijia Lou[a], Alla Zelenyuk[a], Richard C. Easter[a], Richard A. Corley[a], Brian D. Thrall[a], Philip J. Rasch[a], Jerome D. Fast[a], Staci L. Massey Simonich[b,c], Huizhong Shen[d], and Shu Tao[e]

[a]Pacific Northwest National Laboratory, Richland, WA 99352; [b]Department of Chemistry, Oregon State University, Corvallis, OR 97331; [c]Environmental and Molecular Toxicology, Oregon State University, Corvallis, OR 97331; [d]School of Civil & Environmental Engineering, Georgia Institute of Technology, Atlanta, GA 30332; and [e]Laboratory for Earth Surface Processes, College of Urban and Environmental Sciences, Peking University, Beijing 100871, China

Edited by John H. Seinfeld, California Institute of Technology, Pasadena, CA, and approved December 23, 2016 (received for review November 8, 2016)

Polycyclic aromatic hydrocarbons (PAHs) have toxic impacts on humans and ecosystems. One of the most carcinogenic PAHs, benzo(*a*)pyrene (BaP), is efficiently bound to and transported with atmospheric particles. Laboratory measurements show that particle-bound BaP degrades in a few hours by heterogeneous reaction with ozone, yet field observations indicate BaP persists much longer in the atmosphere, and some previous chemical transport modeling studies have ignored heterogeneous oxidation of BaP to bring model predictions into better agreement with field observations. We attribute this unexplained discrepancy to the shielding of BaP from oxidation by coatings of viscous organic aerosol (OA). Accounting for this OA viscosity-dependent shielding, which varies with temperature and humidity, in a global climate/chemistry model brings model predictions into much better agreement with BaP measurements, and demonstrates stronger long-range transport, greater deposition fluxes, and substantially elevated lung cancer risk from PAHs. Model results indicate that the OA coating is more effective in shielding BaP in the middle/high latitudes compared with the tropics because of differences in OA properties (semisolid when cool/dry vs. liquid-like when warm/humid). Faster chemical degradation of BaP in the tropics leads to higher concentrations of BaP oxidation products over the tropics compared with higher latitudes. This study has profound implications demonstrating that OA strongly modulates the atmospheric persistence of PAHs and their cancer risks.

polycyclic aromatic hydrocarbons | organic aerosols | climate model | viscous aerosol shield | heterogeneous chemistry

Polycyclic aromatic hydrocarbons (PAHs) are unavoidable byproducts of any kind of combustion process involving organic matter. Exposure to PAHs is associated with cancer and other health risks (1–3). Among the many PAHs, benzo(*a*)pyrene (BaP) is one of the most highly carcinogenic agents. BaP is used as an indicator of cancer risk from exposure to PAH mixtures (4, 5), and is also a criteria pollutant in many countries.

PAHs are known for their persistence in the atmosphere and their long-range transport far from sources (6–8). Despite decades of research, the mechanisms responsible for the observed atmospheric persistence and long-range transport of PAHs are not well understood, mainly due to incomplete knowledge of gas–particle partitioning and chemical loss rates of PAHs (9). Although gas-phase BaP is rapidly degraded by oxidants such as OH radicals (10–12), most of the gaseous BaP rapidly partitions to atmospheric particulate matter due to its low volatility (12). Therefore, heterogeneous chemical degradation of particle-bound BaP is an important loss mechanism (13–19). Laboratory measurements show that BaP adsorbed on the surface of elemental carbon, solid organic carbon, or ammonium sulfate particles reacts quickly with ozone, and its oxidation lifetime varies from several minutes to a few hours (15, 18, 19). However, field measurements demonstrate that BaP persists longer in the atmosphere and is therefore transported far from its sources (20). Consistently, chemical transport models have suggested that BaP needs to undergo much slower heterogeneous loss to match observations (11, 21, 22). In this study, we demonstrate a key missing link based on recent measurements that mechanistically reconciles model predictions with laboratory and field measurements.

Combining laboratory, field, and modeling results, we develop approaches to represent how temperature- and relative humidity (RH)-dependent variations in effective viscosity of organic aerosol (OA) affect the heterogeneous chemistry of BaP in the atmosphere. We propose three major amendments to the currently inadequate conceptual framework for describing BaP evolution, by (*i*) including laboratory-observed heterogeneous oxidation of particle-bound BaP coated with OA, (*ii*) representing slowing, or complete shutoff of BaP oxidation in cool and/or dry conditions due to shielding by OA coatings, and (*iii*) including the heterogeneous oxidation products of BaP, which are assumed to remain particle-bound rather than being lost, so that they can be transported in the atmosphere and removed by deposition. Although previous measurements mostly focused on uncoated particle-surface-adsorbed BaP directly exposed to ozone, it has been recently shown that coatings of highly viscous secondary organic aerosol (SOA) material can significantly slow the oxidation of particle-bound BaP adsorbed on ammonium sulfate aerosols (19). Coatings of solid organic eicosane have been shown to stop BaP oxidation

Significance

Polycyclic aromatic hydrocarbons (PAHs) adversely impact human health and ecosystems and are known to persist in the atmosphere. Despite decades of research, the mechanisms by which these PAHs persist are not well understood. Here, we combine theory and laboratory and field measurements within a global climate model to produce new insights into mechanisms that are responsible for the observed persistence of PAHs. We show that temperature- and humidity-dependent variations in effective viscosity of organic aerosol (OA) shield PAHs from chemical degradation. This OA shielding results in higher PAH concentrations at both near-urban and remote locations, leading to a fourfold increase in global lung cancer risk. Our study represents new research frontiers in terms of connecting climate-relevant OA with health-relevant PAHs.

Author contributions: M.S. and A.Z. designed research; M.S., S.L., and R.C.E. performed research; M.S. and S.L. analyzed data; and M.S., S.L., A.Z., R.C.E., R.A.C., B.D.T., P.J.R., J.D.F., S.L.M.S., H.S., and S.T. wrote the paper.

The authors declare no conflict of interest.

This article is a PNAS Direct Submission.

[1]To whom correspondence should be addressed. Email: ManishKumar.Shrivastava@pnnl.gov.

This article contains supporting information online at www.pnas.org/lookup/suppl/doi:10.1073/pnas.1618475114/-/DCSupplemental.

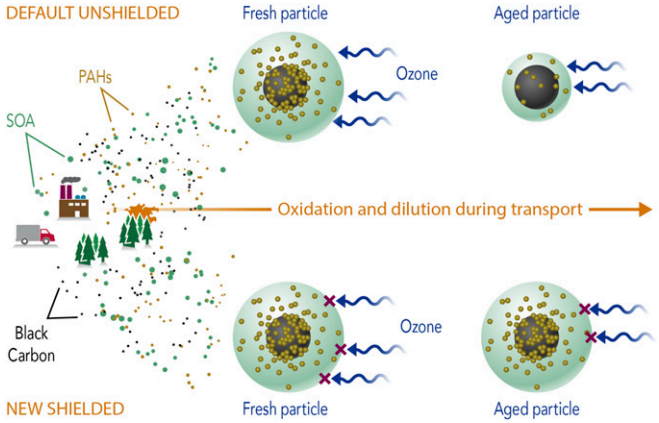

Fig. 1. Schematic comparing the default unshielded (top) and the new shielded (bottom) modeling formulations for PAHs (BaP used in this study). In both formulations, BaP (yellow circles) is either adsorbed on BC (black spherical core) or absorbed in OA (green coating surrounding the core). In the default unshielded formulation, BaP undergoes fast heterogeneous oxidation by ozone, and the liquid-like organic coating can decrease due to evaporation during transport. In the new shielded formulation, a nonvolatile, highly viscous OA coating effectively shields particle-bound BaP from oxidation by ozone in cool and/or dry conditions.

completely (18). Other measurements have demonstrated that heterogeneous oxidation of particle-surface-bound PAHs in the atmosphere decreases substantially due to accumulation of SOA species over particles during their atmospheric transport and chemical aging (23). Heterogeneous reactions of PAHs with ozone are limited mostly to the particle surface, where ozone can be catalytically destroyed (24). Highly viscous SOA coatings limit the diffusion of PAH molecules from particle bulk to particle surface (24, 25), effectively shielding PAHs from chemical degradation (24). In addition, OA is more viscous in cool/dry conditions (24, 26), so the effectiveness of shielding by OA is likely higher at cool locations in the atmosphere compared with laboratory measurements, which are made at room temperature [i.e., around 296° K (18, 19, 25)]. Thus, temperature- and RH-dependent changes in the viscosity of OA coatings can strongly affect heterogeneous oxidation kinetics of BaP.

Here, we include these three amendments to the BaP modeling framework in a global atmospheric chemistry climate model (*Methods*), as illustrated in Fig. 1. A major fraction (generally ≥90%) of freshly emitted gaseous BaP is absorbed within coemitted primary organic aerosol (POA) and subsequently formed SOA, or adsorbed onto coemitted soot/black carbon (BC). At warm/humid conditions, BaP heterogeneous oxidation is assumed to be RH-dependent based on laboratory measurements of BaP coated by SOA (19). At cool and/or dry conditions, however, we assume that highly viscous OA effectively shields BaP from heterogeneous oxidation, similar to that observed for eicosane (a highly viscous solid organic) coatings (18) (*SI Appendix*, *Shielding of BaP by OA in the New Modeling Formulation*). This approach is consistent with highly viscous SOA observed at dry conditions (27, 28), persistence of highly viscous SOA at cooler temperatures in the free troposphere (26), and also higher viscosity of complex SOA mixtures (29) that are likely more atmospherically relevant compared with laboratory-generated SOA (*SI Appendix*, *Shielding of BaP by OA in the New Modeling Formulation*). We show that including the shielding of BaP by OA results in better agreement with BaP measurements in the field, promotes stronger long-range transport, and also produces greater global incremental lung cancer risk (ILCR) estimates due to exposure to PAHs, compared with the default model that neglects this shielding by OA.

Results

We incorporate the two formulations (new, where OA coatings shield BaP from heterogeneous oxidation, and default, where OA does not shield BaP, defined in *SI Appendix*, Table S1) within the global Community Atmosphere Model version 5.2 (CAM5). Simulations are performed for 2007–2010. We use a global BaP emissions inventory from 2008 (30) (*Methods*), and assign temporal and vertical profiles to BaP emissions in relevant source categories (*SI Appendix*, *Temporal and Vertical Profiles of BaP Emissions*). Both SOA and directly emitted POA contribute to the OA coating thickness, but SOA dominates the global budget of OA (31). OA consists of thousands of organic species with different chemical compositions (32) (*SI Appendix*, *Temporal and Vertical Profiles of BaP Emissions, Organic Aerosol (OA) Composition*). Although SOA is treated as liquid-like and semivolatile in the default formulation, the new formulation treats SOA as an effectively nonvolatile highly viscous semisolid, which has been shown to agree with a suite of global OA measurements (31) (*SI Appendix*, *SOA Treatments*). The simulated coating thickness of OA around the BC core is calculated in every model grid and time step and often exceeds the threshold of 20 nm for being classified as a thick coating (*SI Appendix*, *OA Coating Around BC Core*). Model simulated coating thickness is within the range of reported measurements of OA coating thicknesses (33).

Model Predictions and Global BaP Measurements. Because the global model (coarse grid resolution ~200 km) cannot resolve high BaP concentrations near strong urban emissions sources, we first evaluate model predictions with global gas-plus-particle-phase BaP measurements at 69 nonurban (background) sites, globally (site locations are shown in *SI Appendix*, Fig. S1). Fig. 2*A* shows that the default unshielded formulation greatly underpredicts

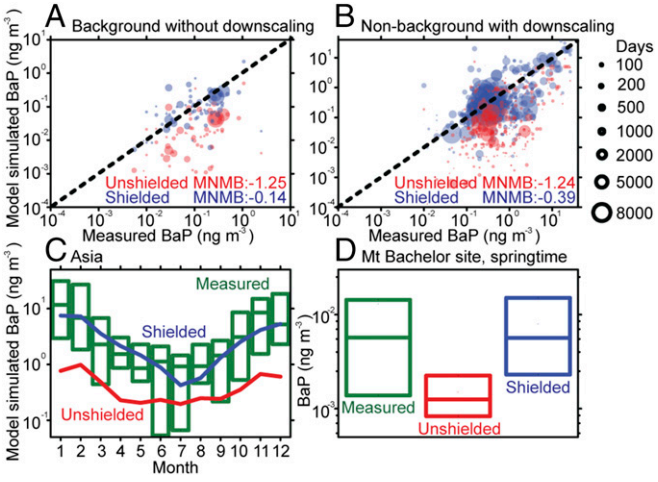

Fig. 2. Evaluation of 2008–2010 near-surface BaP concentration predicted by the default unshielded (red) and new shielded (blue) modeling formulations against field measurements of BaP. Model results for each site are averages over observation days. (*A* and *B*) Scatter plots of simulated and measured concentrations at (*A*) 69 background/remote sites and (*B*) 294 nonbackground sites around the world (22, 49–51). Modified normalized mean biases (MNMB) are calculated as in Wagner et al. (52). Areas of circles are proportional to the number of days sampled at each site. (*C*) Annual variation of measured and simulated BaP concentrations at 18 sites (6 background and 12 nonbackground) in Asia. Green boxes denote measured values (medians and 15th and 85th percentiles of site monthly means), and blue (new shielded model) and red lines (default unshielded model) denote medians of model-simulated site monthly means. (*D*) Measured and simulated BaP concentrations (medians and 15th and 85th percentiles) at the Mount Bachelor Observatory mountain site near the west coast of the United States during spring (March through May) (34).

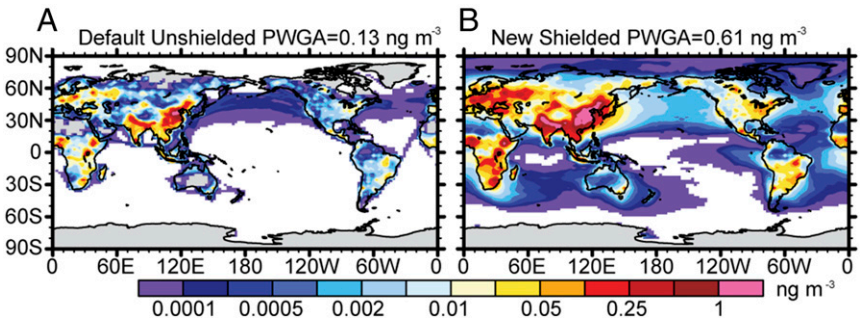

Fig. 3. Simulated (nondownscaled) global near-surface 2008–2010 average particle-bound BaP concentrations (nanograms per cubic meter) predicted by (*A*) the default unshielded and (*B*) the new shielded BaP modeling formulations. White areas are grid cells with BaP concentrations $< 10^{-5}$ ng·m^{-3}. PWGA (at top of each plot) are population-weighted global average concentrations.

measured BaP concentrations (red circles), whereas the new shielded model shows much better agreement (blue circles are closer to the 1:1 line). Consistently, the default formulation shows a large negative modified normalized mean bias (predicted values ∼77% lower than observed), whereas the bias in the new model is only ∼13% lower than observed. However, the coarse-grid global model significantly underestimates concentrations in near-urban regions (*SI Appendix*, Fig. S2). A better estimate of model-predicted concentrations near urban sites is achieved by downscaling calculated concentrations to 0.1° × 0.1° based on emission density, wind speed, frequency, and direction, and gas- and particle-phase BaP oxidation rates (22) (*SI Appendix*, *Global Model Downscaling Formulation*). Fig. 2*B* compares measured and model-predicted concentrations at 294 nonbackground sites (mostly located in cities) around the world after downscaling the near-surface simulated concentrations. Even at these nonbackground sites, the default formulation shows a large negative bias, with simulated values ∼76% lower than observed on average, whereas the new model shows better agreement with measurements (simulated values ∼33% lower than observed). Importantly, most of the larger blue circles are closer to the 1:1 line in Fig. 2*B*, indicating that the new model agrees much better with longer-term (i.e., more reliable) observations.

Fig. 2*C* indicates that, compared with the monthly observed data at 18 sites in Asia (green boxes), the new model (blue line) captures both the magnitude and seasonal variations of BaP concentrations. Both simulated and observed BaP concentrations peak during the winter (December through February), with minima during summer (June through August). Predicted seasonality in BaP concentrations is due to seasonality in both BaP emissions and BaP oxidation rates. Residential biofuel and fossil fuel emissions peak during wintertime in this region, and contribute 78% to BaP emissions during winter and 56% during summer (30). Also, in the new model, lower wintertime temperatures favor complete shielding of BaP due to higher viscosity of OA coating at cooler temperatures (blue shaded area in *SI Appendix*, Fig. S3*B*), whereas BaP is not shielded by OA that is more liquid-like during the summer (orange shaded area in *SI Appendix*, Fig. S3*B*). The default formulation (red line) shows a similar seasonal cycle, but it greatly underpredicts BaP concentrations throughout the year.

Fig. 2*D* compares the measured and simulated (gas-plus-particle-phase) BaP concentrations at Mount Bachelor Observatory, located in the Cascade Range of the northwestern United States about 200 km from the Pacific coast (44°N, 121.7°W, 2,763 m above sea level). This site is impacted by episodic trans-Pacific atmospheric transport during the winter and spring, and is chosen for evaluation of long-range and regional transport of BaP. Fig. 2*D* shows that the new model agrees much better with the measured (34) BaP concentrations at this site during the springtime (March through May), compared with the default. The median simulated new model BaP concentration of 5.7×10^{-3} ng·m^{-3} is same as the observed median of 5.7×10^{-3} ng·m^{-3}, whereas the default formulation predicts a factor of 4.3 lower median BaP concentration compared with the observed value.

The substantially better agreement of our new modeling formulation compared with the default is mainly due to complete shielding by OA at cool and/or dry conditions (*SI Appendix*, *Temperature- and RH-Dependent Shielding of BaP by OA*). To further investigate the sensitivity of simulated BaP to the shielding assumptions of the new formulation, we conducted an additional limited-shielding simulation where we applied the room-temperature laboratory-measured oxidation kinetics of SOA-coated BaP over a wider temperature range, i.e., down to 276° K where measurements are lacking (*SI Appendix*, *Limited-Shielding Treatment* and Fig. S3*C*), compared with 296° K and above in the new modeling formulation. This limited-shielding treatment also showed a large negative model measurement bias, similar to the default formulation (*SI Appendix*, Fig. S4*B*). This result suggests that more complex and aged atmospheric SOA, which is highly viscous at cool/dry conditions (24, 26, 29), is expected to be highly effective in shielding BaP from oxidation, as is assumed in our new modeling formulation.

Global distributions of 2008–2010 annual average near-surface BaP concentrations from the default (unshielded) and new (shielded) modeling formulations are shown in Fig. 3 *A* and *B*, respectively. Simulated BaP concentrations vary widely, with concentrations exceeding 0.1 ng·m^{-3} (red and pink areas in Fig. 3) over major source regions in Asia, Europe, Russia, and Africa. The World Health Organization (WHO) suggests a human health-based guideline of 0.1 ng·m^{-3}, and indicates that a lifetime exposure to 0.1 ng·m^{-3} of BaP (as an indicator of the total PAH concentration) would theoretically lead to one extra cancer case in 100,000 exposed individuals (4). Fig. 3 indicates that, unlike the default (unshielded) formulation, the new model frequently produces concentrations that exceed the WHO guideline for BaP, especially over parts of East and South Asia, Africa, and Europe. Also, at several locations, the new (shielded) model predicts an order-of-magnitude-higher BaP concentration compared with the default (unshielded) formulation. Downscaling global BaP concentrations increases global population-weighted average BaP concentrations by a factor of ∼2 (*SI Appendix*, Fig. S5), with larger increases regionally.

Lung Cancer Risk Assessment. BaP can be used as an indicator of risk due to exposure to all PAH mixtures (not just BaP), using a method based on epidemiological data (4). We calculate an unbiased best estimate of ILCR as described by Shen et al. (22) (*SI Appendix*, *Incremental Lifetime Cancer Risk*), due to exposure to PAHs using globally downscaled BaP concentrations (*SI Appendix*, Fig. S5). Fig. 4 shows that the new shielded formulation predicts a global population-weighted average ILCR of 2×10^{-5}, which exceeds the acceptable limit of 1×10^{-5} (i.e., 1 death per 100,000 individuals), whereas the default unshielded formulation predicts a global ILCR of 0.6×10^{-5} that is within the acceptable risk levels due to PAH exposure. Consistent with our new model predictions, another global modeling study (22) predicted a global population-weighted ILCR of 3×10^{-5}, but that study completely omitted the heterogeneous oxidation kinetics of BaP. Heterogeneous oxidation

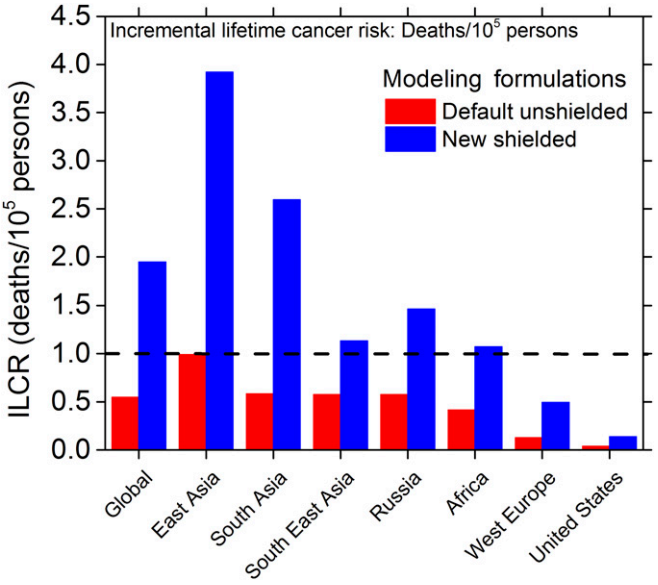

Fig. 4. Global and regional population-weighted ILCR for PAH mixtures calculated for the default unshielded (red) and new shielded (blue) modeling formulations using 0.1° × 0.1° downscaled BaP concentrations, as described in *SI Appendix*. Bars that are higher than the dashed line represent significant lung cancer risks of humans due to exposure to PAH mixtures. BaP is used as a reference for total PAH ILCR calculations.

is an important global sink of BaP in both the default and new modeling formulations in this study, consistent with measurements, and also has important implications as discussed in *Heterogeneous Oxidation Products of BaP*. The new modeling formulation also predicts the highest ILCR in East Asia (4×10^{-5}), and elevated ILCR in other regions including South Asia, most of which is in India (2.6×10^{-5}), Russia (1.5×10^{-5}) and Africa (1.1×10^{-5}). In contrast, the default formulation suggests a factor of ∼3 to 4 lower cancer risk in these regions, which is below the threshold of 1×10^{-5} for acceptable risk (Fig. 4). Both formulations predict low and insignificant ILCR in the United States, which only accounts for 2% of the global BaP emissions (30).

Lifetime and Long-Range Transport of BaP. The default unshielded formulation predicts a very short lifetime of BaP (∼2 h), due to heterogeneous oxidation by ozone (calculated as ratio of global burden of BaP to its heterogeneous oxidation sink), and also greatly underpredicts global measurements of BaP (Fig. 2). In contrast, the new shielded formulation predicts a much longer BaP oxidation lifetime of ∼5 d, which is similar to the removal timescale for BaP associated with wet and dry removal processes. This increase in oxidation lifetime from hours to days results in much stronger atmospheric long-range transport.

To demonstrate the consequences of atmospheric long-range transport of BaP, we conduct several additional simulations in which BaP emissions from different source regions are turned on in the model, one at a time. Fig. 5 compares the long-range transport of BaP emitted from three major regions, East Asia, Western Europe, and Africa, which together comprise 63% of global BaP emissions. The new shielded model (Fig. 5, *Top*) clearly shows much farther long-range transport of BaP compared with the default unshielded formulation (Fig. 5, *Bottom*). For example, BaP emitted from East Asia travels thousands of miles over the Pacific Ocean, reaching the west coast of the United States, consistent with previous observational studies that identified trans-Pacific atmospheric transport of PAHs (34–36). Similarly, BaP emitted from Western Europe travels to the east, and BaP emitted from South Africa travels over the South Atlantic Ocean, reaching South America. In sharp contrast, the default unshielded formulation (Fig. 5, *Bottom*) predicts much weaker long-range transport, and most BaP is localized over respective emissions source regions. Similar differences in the long-range transport potential of BaP between the new shielded and default unshielded modeling formulations are also seen for other source regions, including South Asia (including India), Southeast Asia, and Russia (*SI Appendix*, Fig. S6).

Although BaP emissions are the same in the new and default models, the new model predicts a factor of ∼9 larger deposition flux of BaP (i.e., combined wet and dry deposition to Earth's surface), compared with the default (*SI Appendix*, *Dry and Wet Deposition of BaP* and Fig. S7) because, in the default model, BaP undergoes much faster chemical degradation. In both formulations, a major fraction of BaP (77 to 90%) is deposited over land (*SI Appendix*, Fig. S7), but significantly more BaP persists, and is transported and deposited in oceans in the new shielded (22%), compared with the default (10%), modeling formulation, which could have ecological implications (37).

Heterogeneous Oxidation Products of BaP. Previous modeling studies have primarily assumed that PAHs that undergo heterogeneous oxidation in the atmosphere are completely degraded (11, 21, 38). However, recent experimental studies show that several oxidized PAHs could remain particle-bound, and often appear as higher molecular weight peaks in particle mass spectra (25, 39). Some oxidized BaP species have been shown to be toxic (40), and some are direct-acting mutagens (39); therefore, it is important to quantify their atmospheric exposure. Here, we track the oxidation

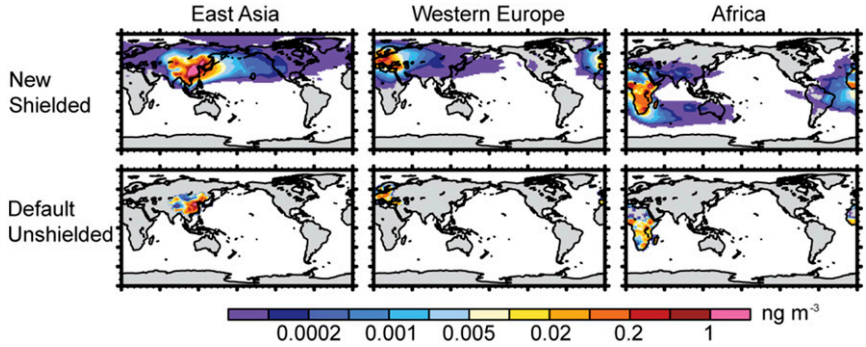

Fig. 5. Simulated near-surface 2008-annual average concentrations of BaP from three major source regions: East Asia (*Left*), Western Europe (*Center*) and Africa (*Right*) for new shielded (*Top*) and the default unshielded (*Bottom*) modeling formulations, as indicators of long-range transport potential. BaP emissions are only turned on for the respective source regions with emissions over the rest of the globe turned off. White areas are grid cells with BaP concentrations < 10^{-5} ng·m^{-3}.

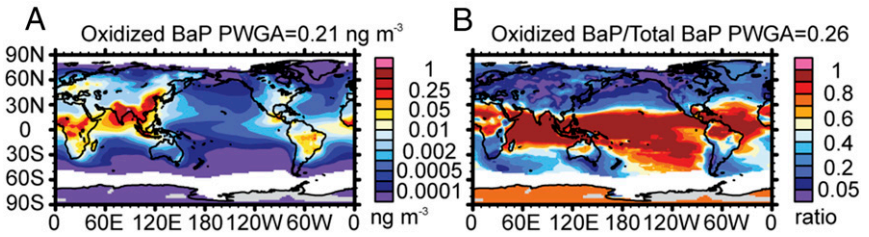

Fig. 6. New shielded model-predicted BaP oxidation products. (*A*) Near-surface 2008–2010 annual average concentrations of BaP oxidation products. (*B*) Fraction of total (fresh+oxidized) BaP that is oxidized. PWGA (above each plot) are population-weighted global averages. White areas are grid cells with oxidized/total BaP concentrations < 10^{-5} ng·m^{-3}.

products of particle-bound BaP using a separate oxidized BaP tracer species in the model. This oxidized BaP tracer is assumed to be particle-bound, nonvolatile, and nonreactive, and represents the sum of all potential oxidation products of BaP, most of which are not routinely measured. The new (shielded) formulation predicts that oxidized BaP concentrations could be as high as fresh BaP concentrations over several regions globally (Figs. 6*A* and 3*B*), and could be important for BaP exposure assessment. Fig. 6*B* shows that, on a global population-weighted basis, oxidized BaP constitutes ~26% of total (fresh+oxidized) BaP. However, over the tropics (30°S to 30°N), more than 80% of the total particle-bound BaP is converted to oxidized BaP due to heterogeneous oxidation by ozone (Fig. 6*B*). The tropics are characterized by high temperature and high RH conditions (*SI Appendix*, Fig. S8), which reduce the effectiveness of shielding by OA (*SI Appendix*, Fig. S3*B*), because, under these conditions, OA becomes less viscous (liquid-like) (27, 28). Model-predicted spatial differences in the ratio of oxidized to total BaP between the tropics and high/middle latitudes (Fig. 6*B*) reflect differences in the shielding effects of OA, consistent with semisolid (highly viscous) particles observed over boreal forests and liquid particles (less viscous) observed over tropical forests (41, 42). In comparison with the new formulation, the default unshielded formulation results in fast heterogeneous oxidation of particle-bound BaP, because BaP is always available to react with ozone (*SI Appendix*, Fig. S3*A*). Therefore, in the default formulation, most of the BaP (~85%) is rapidly oxidized and converted to oxidized BaP throughout the globe (*SI Appendix*, Fig. S9*B*), but this is inconsistent with fresh BaP measurements, as discussed earlier (Fig. 2).

Discussion

This work has several implications for understanding the atmospheric persistence, long-range transport, deposition, and health impacts of PAHs. Most previous models including heterogeneous oxidation of BaP (11, 20, 21) have noted large discrepancies between modeled and measured BaP concentrations. Our study shows that shielding of particle-bound BaP by OA coatings can reconcile these discrepancies, producing a realistic and physically consistent picture of BaP evolution. Our study suggests that this mechanistic interaction between climate-relevant OA and health-relevant PAHs should be explicitly represented in PAH chemical transport models. We show that the OA coating is likely more effective in shielding PAHs in the middle/high latitudes compared with the tropics because of differences in OA properties [semisolid when cool/dry (42–44) vs. liquid-like when warm/humid, as shown by OA measurements (27, 28)]. Thus, the effectiveness of shielding depends on the viscosity of OA that varies with temperature, RH, and the atmospheric aging of complex OA coatings. This viscosity-dependent shielding needs to be better constrained by future laboratory and field measurements.

Another important implication of the variable effectiveness of shielding by OA is reflected in the predicted atmospheric concentrations of BaP oxidation products, which, previously, have not been explicitly modeled. The larger fraction of BaP oxidation products over the tropics is a direct consequence of reduced shielding by OA at these high temperature/high humidity locations.

Methods

Model Setup. We develop and incorporate new PAH modules into the global CAM5, and perform simulations at a grid spacing of 1.9° × 2.5° with 30 vertical levels between the surface and 3.6 hPa. Horizontal winds and temperature are nudged toward the European Centre for Medium-Range Weather Forecasts reanalysis-Interim (ERA-Interim) reanalysis data (45), with relaxation times of 6 h and 24 h, respectively. Simulations are conducted for 2007–2010, with the first year used for initialization and model spin-up. We use the Model for Ozone and Related Chemical Tracers (MOZART-4) gas-phase chemistry mechanism and the three-mode version of the Modal Aerosol Model (MAM3), with changes to both SOA and its precursor gases (*SI Appendix, Temporal and Vertical Profiles of BaP Emissions, BC, POA and SOA Precursor Gas Emissions*), as described in detail by Shrivastava et al. (31).

BaP Emissions. We use the 0.1° × 0.1° global PAH emissions inventory (30) for BaP, available at www.ues.pku.edu.cn/inventory/home.html. This inventory provides total annual BaP emissions within each grid cell, without any vertical/temporal distribution information. We assign BaP emissions to fossil fuel and biofuel sectors and distribute them temporally and vertically in the model using OC emissions from respective sectors, as discussed in *SI Appendix, Temporal and Vertical Profiles of BaP Emissions*.

BaP Gas–Particle Partitioning. Gas–particle partitioning of PAHs is described by various theoretical/empirical models based on single-parameter or poly-parameter linear free energy relationships (sp- or pp-LFER) (46). The sp-LFER models, which relate the partitioning constant for PAH to OA or BC to just one thermodynamic property (e.g., subcooled liquid vapor pressure of PAHs), have often been used in regional and global atmospheric chemistry models to predict gas–particle partitioning of PAHs (11, 22). In comparison, the pp-LFER models relate partitioning constant to more than one property, and thus account for all significant interactions between solute and sorbent (46). In this study, we implement the pp-LFER model to calculate partitioning of PAHs by adsorption to BC and absorption into OA, similar to Shahpoury et al. (46).

We also develop a new algorithm to treat gas–particle partitioning of PAHs simultaneously to various aerosol modes of MAM3 (47) in CAM5 (*SI Appendix, Algorithm for Gas–Particle Partitioning of PAHs to Modal Aerosols*).

BaP Gas–Phase Reactions. Gas-phase reaction of BaP with the hydroxyl radical (OH) is included. The second-order rate coefficient for reactions of BaP with OH is set as 5×10^{-11} cm^3 per molecule per second (11, 12).

BaP Particle-Phase Heterogeneous Reactions. We also include heterogeneous reactions of particle-phase BaP with ozone and OH radicals (12, 18, 19). We assume a constant second-order heterogeneous reaction rate constant with OH radicals (2.9×10^{-13} cm^3 per molecule per second) (48). Note that this reaction rate is about two orders of magnitude slower than the gas-phase reaction rate of BaP with OH radicals. However, heterogeneous oxidation kinetics of BaP with ozone can be much faster under certain conditions. Ozone reaction kinetics for BaP are included using the Langmuir–Hinselwood mechanism, indicating a surface reaction between particle-borne BaP and ozone (18, 19). In addition, as described in *SI Appendix*, shielding of BaP by OA can reduce or, under certain conditions, completely stop the BaP particle-phase heterogeneous reactions.

ACKNOWLEDGMENTS. The research described in this paper was conducted under the Laboratory Directed Research and Development Program at Pacific Northwest National Laboratory (PNNL), a multiprogram national laboratory operated by Battelle for the US Department of Energy (DOE). This research was also supported by the Environmental Molecular Science Laboratory (EMSL), a US DOE Office of Science user facility sponsored by the US DOE's Office of Biological and Environmental Research and located at PNNL. The PNNL Institutional Computing (PIC) program and EMSL provided computational resources for the model simulations. The Community Earth System Model (CESM) project is supported by the National Science Foundation and the Office of Science of the DOE. The Pacific Northwest National Laboratory is operated for the US DOE by Battelle Memorial Institute under contract DE-AC05-76RL01830. R.C. and S.L.M.S. were supported by the National Institute of Environmental Health Sciences (NIEHS) through grant numbers P30ES00210 and P42ES016465. S.L.M.S. was also supported by the National Science Foundation (NSF) through grant number AGS-11411214. A.Z. was supported by the US DOE Office of Science, Office of Basic Energy Sciences (BES), Division of Chemical Sciences, Geosciences and Biosciences. P.J.R. was supported by the US DOE, Office of Science, Biological and Environmental Research program as part of the Earth System Modeling Program. Part of the BaP measurements data used in this research were provided by Jana Borůvková, carried out with the support of core facilities of RECETOX Research Infrastructure, project number LM2015051, funded by the Ministry of Education, Youth and Sports of the Czech Republic and LO1214 (National Sustainability Programme).

1. Boffetta P, Jourenkova N, Gustavsson P (1997) Cancer risk from occupational and environmental exposure to polycyclic aromatic hydrocarbons. *Cancer Causes Control* 8(3):444–472.
2. Chen SC, Liao CM (2006) Health risk assessment on human exposed to environmental polycyclic aromatic hydrocarbons pollution sources. *Sci Total Environ* 366(1):112–123.
3. Perera FP (1997) Environment and cancer: Who are susceptible? *Science* 278(5340): 1068–1073.
4. Boström CE, et al. (2002) Cancer risk assessment, indicators, and guidelines for polycyclic aromatic hydrocarbons in the ambient air. *Environ Health Perspect* 110(Suppl 3):451–488.
5. Delgado-Saborit JM, Stark C, Harrison RM (2011) Carcinogenic potential, levels and sources of polycyclic aromatic hydrocarbon mixtures in indoor and outdoor environments and their implications for air quality standards. *Environ Int* 37(2):383–392.
6. Lunde G, Bjorseth A (1977) Polycyclic aromatic hydrocarbons in long-range transported aerosols. *Nature* 268(5620):518–519.
7. Macdonal RW, et al. (2000) Contaminants in the Canadian Arctic: 5 years of progress in understanding sources, occurrence and pathways. *Sci Total Environ* 254(2-3):93–234.
8. Sofowote UM, et al. (2011) Assessing the long-range transport of PAH to a sub-Arctic site using positive matrix factorization and potential source contribution function. *Atmos Environ* 45(4):967–976.
9. Lammel G, et al. (2015) Long-range atmospheric transport of polycyclic aromatic hydrocarbons is worldwide problem—Results from measurements at remote sites and modelling. *Acta Chim Slov* 62(3):729–735.
10. Finlayson-Pitts BJ, Pitts JN (2000) *Chemistry of the Upper and Lower Atmosphere: Theory, Experiments and Applications* (Academic, New York).
11. Friedman CL, Selin NE (2012) Long-range atmospheric transport of polycyclic aromatic hydrocarbons: A global 3-D model analysis including evaluation of Arctic sources. *Environ Sci Technol* 46(17):9501–9510.
12. Keyte IJ, Harrison RM, Lammel G (2013) Chemical reactivity and long-range transport potential of polycyclic aromatic hydrocarbons—A review. *Chem Soc Rev* 42(24): 9333–9391.
13. Ringuet J, Albinet A, Leoz-Garziandia E, Budzinski H, Villenave E (2012) Reactivity of polycyclic aromatic compounds (PAHs, NPAHs and OPAHs) adsorbed on natural aerosol particles exposed to atmospheric oxidants. *Atmos Environ* 61:15–22.
14. Kahan TF, Kwamena NOA, Donaldson DJ (2006) Heterogeneous ozonation kinetics of polycyclic aromatic hydrocarbons on organic films. *Atmos Environ* 40(19):3448–3459.
15. Kwamena NOA, Thornton JA, Abbatt JPD (2004) Kinetics of surface-bound benzo[*a*]pyrene and ozone on solid organic and salt aerosols. *J Phys Chem A* 108(52):11626–11634.
16. Liu C, Zhang P, Yang B, Wang Y, Shu J (2012) Kinetic studies of heterogeneous reactions of polycyclic aromatic hydrocarbon aerosols with NO_3 radicals. *Environ Sci Technol* 46(14):7575–7580.
17. Poschl U, Letzel T, Schauer C, Niessner R (2001) Interaction of ozone and water vapor with spark discharge soot aerosol particles coated with benzo[*a*]pyrene: O_3 and H_2O adsorption, benzo[*a*]pyrene degradation, and atmospheric implications. *J Phys Chem A* 105(16):4029–4041.
18. Zhou S, Lee AKY, McWhinney RD, Abbatt JPD (2012) Burial effects of organic coatings on the heterogeneous reactivity of particle-borne benzo[*a*]pyrene (BaP) toward ozone. *J Phys Chem A* 116(26):7050–7056.
19. Zhou S, Shiraiwa M, McWhinney RD, Pöschl U, Abbatt JPD (2013) Kinetic limitations in gas-particle reactions arising from slow diffusion in secondary organic aerosol. *Faraday Discuss* 165:391–406.
20. Lohmann R, Lammel G (2004) Adsorptive and absorptive contributions to the gas-particle partitioning of polycyclic aromatic hydrocarbons: State of knowledge and recommended parametrization for modeling. *Environ Sci Technol* 38(14):3793–3803.
21. Sehili AM, Lammel G (2007) Global fate and distribution of polycyclic aromatic hydrocarbons emitted from Europe and Russia. *Atmos Environ* 41(37):8301–8315.
22. Shen H, et al. (2014) Global lung cancer risk from PAH exposure highly depends on emission sources and individual susceptibility. *Sci Rep* 4:6561.
23. Jariyasopit N, et al. (2014) Heterogeneous reactions of particulate matter-bound PAHs and NPAHs with NO_3/N_2O_5, OH radicals, and O_3 under simulated long-range atmospheric transport conditions: Reactivity and mutagenicity. *Environ Sci Technol* 48(17):10155–10164.
24. Berkemeier T, et al. (2016) Ozone uptake on glassy, semi-solid and liquid organic matter and the role of reactive oxygen intermediates in atmospheric aerosol chemistry. *Phys Chem Chem Phys* 18(18):12662–12674.
25. Zelenyuk A, et al. (2012) Synergy between secondary organic aerosols and long-range transport of polycyclic aromatic hydrocarbons. *Environ Sci Technol* 46(22):12459–12466.
26. Järvinen E, et al. (2016) Observation of viscosity transition in α-pinene secondary organic aerosol. *Atmos Chem Phys* 16(7):4423–4438.
27. Bateman AP, Bertram AK, Martin ST (2015) Hygroscopic influence on the semisolid-to-liquid transition of secondary organic materials. *J Phys Chem A* 119(19):4386–4395.
28. Renbaum-Wolff L, et al. (2013) Viscosity of α-pinene secondary organic material and implications for particle growth and reactivity. *Proc Natl Acad Sci USA* 110(20): 8014–8019.
29. Abramson E, Imre D, Beránek J, Wilson J, Zelenyuk A (2013) Experimental determination of chemical diffusion within secondary organic aerosol particles. *Phys Chem Chem Phys* 15(8):2983–2991.
30. Shen H, et al. (2013) Global atmospheric emissions of polycyclic aromatic hydrocarbons from 1960 to 2008 and future predictions. *Environ Sci Technol* 47(12):6415–6424.
31. Shrivastava M, et al. (2015) Global transformation and fate of SOA: Implications of low-volatility SOA and gas-phase fragmentation reactions. *J Geophys Res Atmos* 120(9):4169–4195.
32. Hallquist M, et al. (2009) The formation, properties and impact of secondary organic aerosol: Current and emerging issues. *Atmos Chem Phys* 9(14):5155–5236.
33. Forrister H, et al. (2015) Evolution of brown carbon in wildfire plumes. *Geophys Res Lett* 42(11):4623–4630.
34. Primbs T, et al. (2008) Influence of Asian and Western United States urban areas and fires on the atmospheric transport of polycyclic aromatic hydrocarbons, polychlorinated biphenyls, and fluorotelomer alcohols in the Western United States. *Environ Sci Technol* 42(17):6385–6391.
35. Genualdi SA, et al. (2009) Trans-Pacific and regional atmospheric transport of polycyclic aromatic hydrocarbons and pesticides in biomass burning emissions to western North America. *Environ Sci Technol* 43(4):1061–1066.
36. Killin RK, Simonich SL, Jaffe DA, DeForest CL, Wilson GR (2004) Transpacific and regional atmospheric transport of anthropogenic semivolatile organic compounds to Cheeka Peak Observatory during the spring of 2002. *J Geophys Res Atmos* 109(D23): D23S15.
37. Alonso E, et al. (2008) A model for estimating the potential biomagnification of chemicals in a generic food web: Preliminary development. *Environ Sci Pollut Res Int* 15(1):31–40.
38. Matthias V, Aulinger A, Quante M (2009) CMAQ simulations of the benzo(a)pyrene distribution over Europe for 2000 and 2001. *Atmos Environ* 43(26):4078–4086.
39. Jariyasopit N, et al. (2014) Novel nitro-PAH formation from heterogeneous reactions of PAHs with NO_2, NO_3/N_2O_5, and OH radicals: Prediction, laboratory studies, and mutagenicity. *Environ Sci Technol* 48(1):412–419.
40. Knecht AL, et al. (2013) Comparative developmental toxicity of environmentally relevant oxygenated PAHs. *Toxicol Appl Pharmacol* 271(2):266–275.
41. Bateman AP, et al. (2016) Sub-micrometre particulate matter is primarily in liquid form over Amazon rainforest. *Nat Geosci* 9(1):34–37.
42. Virtanen A, et al. (2010) An amorphous solid state of biogenic secondary organic aerosol particles. *Nature* 467(7317):824–827.
43. Saukko E, et al. (2012) Humidity-dependent phase state of SOA particles from biogenic and anthropogenic precursors. *Atmos Chem Phys* 12(16):7517–7529.
44. Vaden TD, Imre D, Beránek J, Shrivastava M, Zelenyuk A (2011) Evaporation kinetics and phase of laboratory and ambient secondary organic aerosol. *Proc Natl Acad Sci USA* 108(6):2190–2195.
45. Dee DP, et al. (2011) The ERA-Interim reanalysis: Configuration and performance of the data assimilation system. *Q J R Meteorol Soc* 137(656):553–597.
46. Shahpoury P, et al. (2016) Evaluation of a conceptual model for gas-particle partitioning of polycyclic aromatic hydrocarbons using polyparameter linear free energy relationships. *Environ Sci Technol* 50(22):12312–12319.
47. Liu X, et al. (2012) Toward a minimal representation of aerosols in climate models: Description and evaluation in the Community Atmosphere Model CAM5. *Geosci Model Dev* 5(3):709–739.
48. Esteve W, Budzinski H, Villenave E (2006) Relative rate constants for the heterogeneous reactions of NO_2 and OH radicals with polycyclic aromatic hydrocarbons adsorbed on carbonaceous particles. Part 2: PAHs adsorbed on diesel particulate exhaust SRM 1650a. *Atmos Environ* 40(2):201–211.
49. Borůvková J, et al. (2015) *GENASIS—Global Environmental Assessment and Information System, Version 2.0* (Masaryk Univ, Brno, Czech Republic). Available at www.genasis.cz. Accessed August 1, 2016.
50. Torseth K, et al. (2012) Introduction to the European Monitoring and Evaluation Programme (EMEP) and observed atmospheric composition change during 1972–2009. *Atmos Chem Phys* 12(12):5447–5481.
51. Galarneau E, Bidleman TF, Blanchard P (2006) Seasonality and interspecies differences in particle/gas partitioning of PAHs observed by the Integrated Atmospheric Deposition Network (IADN). *Atmos Environ* 40(1):182–197.
52. Wagner A, et al. (2015) Evaluation of the MACC operational forecast system—Potential and challenges of global near-real-time modelling with respect to reactive gases in the troposphere. *Atmos Chem Phys* 15(24):14005–14030.